

Repurposing Adversarial Perturbations for Continual Learning: From Defense to Active Alignment

Ran Liu^{1,2}, Min Yu^{1,2*}, Mingqi Liu¹, Jianguo Jiang^{1,2},
Gang Li³, Rongsheng Li⁴, Ning Li¹, Zhen Xu^{1,2}, Weiqing Huang^{1,2}, Ming Liu^{3†}

¹Institute of Information Engineering, Chinese Academy of Sciences

²School of Cyber Security, University of Chinese Academy of Sciences

³Deakin University ⁴Harbin Engineering University

liuran@iie.ac.cn, yumin@iie.ac.cn, m.liu@deakin.edu.au

Abstract

In dynamic environments, large language models need to keep adapting to new tasks, but continual learning often suffers from forgetting, limited transfer, and vulnerability to adversarial perturbations. To address this, we present AdvCL, which repurposes adversarial perturbations as a geometric control signal for stable continual adaptation. AdvCL combines three plug-in modules: Intra-Smooth promotes local smoothness via small adversarial perturbations; Proto-Clip uses similarity clipping to prevent excessive alignment to current task prototype; and Inter-Align applies directional alignment toward previous task prototype to reduce representational gaps. Experiments show consistent gains in both standard performance and robustness, with lower forgetting and stronger transfer. We further analyze key mechanisms by quantifying the sensitivity of Intra-Smooth to perturbation settings and the effect of Inter-Align on task similarity and geometric distance. In summary, the modules provide complementary gains when combined, and each can also be integrated individually into diverse CL paradigms, including replay, regularization, and dynamic architectures, thereby offering a geometric control mechanism for continual learning.

1 Introduction

In dynamic environments, large language models (LLMs) must continually adapt to new tasks while preserving prior capabilities. Parameter efficient fine tuning (PEFT) supports this setting by updating only a small set of parameters (Lester et al., 2021; Hu et al., 2022), and is widely used in continual learning (CL). However, alignment does not ensure stable later adaptation. Models can exhibit rebound, where further fine tuning pulls behavior

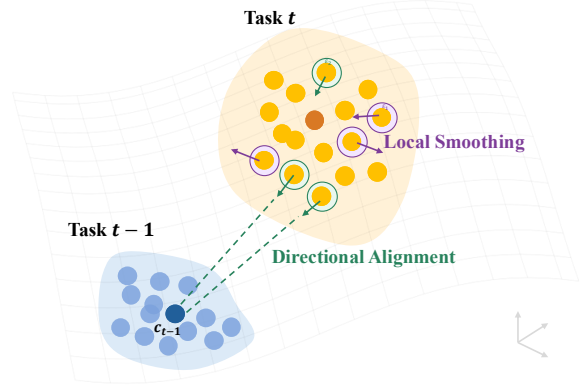


Figure 1: Illustration of local smoothing and directional alignment in representation space.

back toward the pretraining distribution (Ji et al., 2025). This instability aligns with an optimization geometry view, since sharp minima are more sensitive to perturbations and tend to generalize unstably (Keskar et al., 2017), thereby amplifying drift and increasing vulnerability to noise and adversarial inputs. These issues can be traced to unstable representations and insufficiently smooth local geometry, which often manifest as forgetting, rebound, and brittleness.

This motivates a key question: can adversarial perturbations be repurposed from defense into a geometric control signal for stable transfer in CL? The intuition is that robustness reflects local geometric stability, which is tied to mitigating forgetting. Translating this intuition into a practical method is challenging. First, adversarial training involves a trade-off between neighborhood stability and standard accuracy (Zhang et al., 2019), and continual updates can disrupt this stability so that robustness degrades over time (Ru et al., 2024). Second, task similarity strongly influences transfer and forgetting (Hiratani, 2024). Prior work characterizes task relationships to predict transfer feasibility (Achille et al., 2019). But for low similarity task pairs, mainstream methods mainly constrain

*Corresponding author.

†Corresponding author.

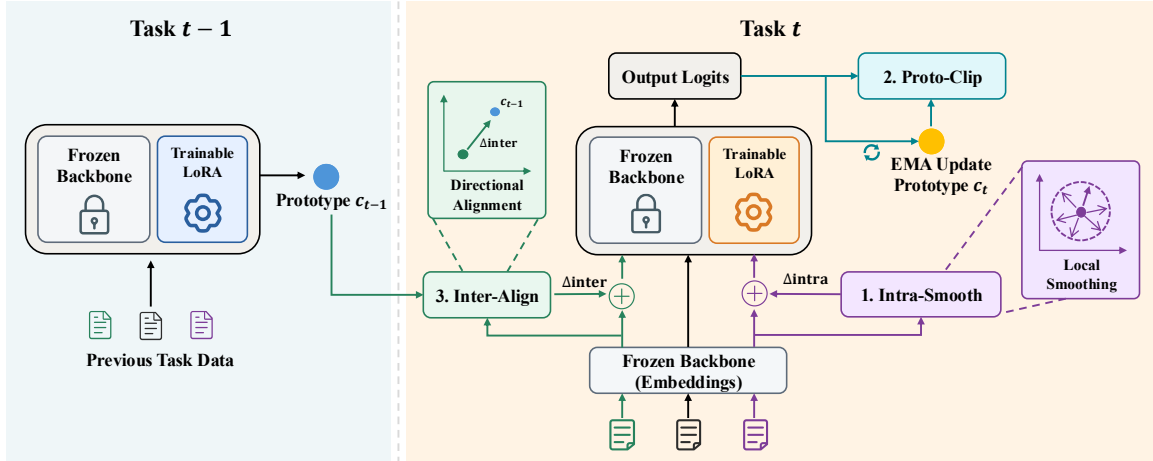


Figure 2: Overview of AdvCL. It integrates Intra-Smooth, Proto-Clip, and Inter-Align, and maintains a prototype for each task as a semantic anchor for similarity clipping and subsequent directional alignment.

drift to preserve old representations (Rebuffi et al., 2017; Cha et al., 2021) instead of actively narrowing cross-task distances.

We argue that adversarial perturbations are valuable because their direction is controllable. As illustrated in Figure 1, they support local smoothing to reduce geometric brittleness (Miyato et al., 2019; Foret et al., 2021) and directional alignment to actively shrink geometric distances between low similarity tasks, thereby improving transfer.

To this end, we present AdvCL, a multi-level adversarial perturbation framework for CL, shown in Figure 2. AdvCL maintains a prototype for the previous task and updates the current prototype with an exponential moving average. It includes three modules: (1) Intra-Smooth, which promotes local smoothing via small perturbations in a frozen embedding neighborhood; (2) Proto-Clip, which clips the similarity between current batch representations and current task prototype to prevent over-alignment toward prototype; and (3) Inter-Align, which performs directional alignment by perturbing features toward the previous prototype, actively shrinking geometric distance between tasks.

Experiments show that AdvCL improves both standard performance and robustness under multiple evaluations, with lower forgetting and stronger transfer. We also find strong transferability of three modules, with complementary gains when combined. Finally, we analyze key mechanisms, including the sensitivity of Intra-Smooth to perturbation solvers and the effect of Inter-Align on task similarity and geometric distance.

Our main contributions are as follows:

(1) We introduce a new CL perspective that treats adversarial perturbations as a tool for local smoothing and cross-task directional alignment, providing a geometric route to improve stability and reduce forgetting. To our knowledge, this is the first to do so in PEFT-CL.

(2) We present AdvCL, a three-module framework that leverages neighborhood perturbations for local smoothing, similarity clipping to avoid over-alignment to the current prototype, and directional alignment for retention and cross-task stability.

(3) AdvCL jointly improves standard performance and robustness, yielding lower forgetting and stronger knowledge transfer. Moreover, modules are applicable to representative CL paradigms.

2 Related Work

Continual learning (CL) mitigates catastrophic forgetting via replay (Rebuffi et al., 2017; Huang et al., 2024), regularization (Kirkpatrick et al., 2017; Wang and Huang, 2024), and dynamic architectures (Rusu et al., 2016; Wang et al., 2024). Parameter efficient fine tuning (PEFT) reduces training cost by updating only a small set of parameters (Houlsby et al., 2019; Hu et al., 2022). Recent PEFT-CL methods largely follow two directions: constraining PEFT updates in a subspace to reduce cross-task conflicts (Wang et al., 2023; Lu et al., 2025), or maintaining a module pool and composing modules via selection or routing to balance stability and plasticity (Zhao et al., 2024; Han et al., 2025). In contrast, we enforce local smoothness via representation space perturbations, making PEFT updates more robust to perturbations and task distri-

bution shifts, thus stabilizing continual adaptation.

Representation space perturbations have been studied for local smoothing and geometric regularization, for example through adversarial training that searches for worst-case directions (Zhu et al., 2020; Jiang et al., 2020) or through noise injection during forward pass (Aghajanyan et al., 2021; Jain et al., 2024). These methods mainly target single task generalization or offline adaptation, not cross-task consistency in CL. They often allow trainable embeddings or full parameter updates, which can drift semantic reference frame so that perturbations across tasks are no longer defined under the same reference frame, amplifying semantic anchor shifts and forgetting. In contrast, we fix embeddings and backbone representations, and use perturbations to enforce local smoothness and improve drift resistance of PEFT subspace updates rather than primarily targeting input robustness.

Task similarity strongly affects transfer and forgetting in CL. Prior work exploits task relations, for example by using task embeddings to measure similarity (Achille et al., 2019) and by selecting task orders (Bell and Lawrence, 2022). Another line stabilizes representations across tasks by anchoring prior knowledge with prototypes, representation alignment, or consistency learning (Cui et al., 2021; Wang et al., 2019; Zhao et al., 2022). Instead of treating similarity as a fixed signal or using alignment only to preserve old representations, we connect the two. Our active alignment paradigm uses similarity to trigger directional alignment on current data toward prior semantic anchors, shrinking representational gaps for low similarity task pairs and improving retention and backward transfer.

3 AdvCL Framework

AdvCL (as illustrated in Figure 2) repurposes adversarial perturbations and auxiliary constraints as training signals, where Intra-Smooth enforces intra-task neighborhood consistency to promote local smoothing, Proto-Clip uses a prototype constraint to prevent over-alignment to current task, and Inter-Align encourages inter-task directional alignment to enhance retention and stability.

3.1 Definitions

We consider online continual learning over a task sequence $\{\mathcal{T}_t\}_{t=1}^N$, where task t has dataset $D_t = \{(x, y)\}$. A single model is trained sequentially

across tasks. At each task, only trainable parameters θ in parameter-efficient fine-tuning (PEFT) modules are updated while backbone parameters remain frozen. We write the model with trainable parameters θ as f_θ , and denote its intermediate representations by $H_\theta(\cdot)$.

Given an input text $x = (w_1, \dots, w_L)$, let $E(x) \in \mathbb{R}^{L \times d_e}$ be its embedding matrix, where d_e is the embedding dimension. We use last layer token representations $H_\theta(x) \in \mathbb{R}^{L \times d}$ to form a text representation via mean pooling:

$$h_\theta(x) = \text{MeanPool}(H_\theta(x)) \in \mathbb{R}^d.$$

We measure similarity using cosine similarity, defined as:

$$S(\mathbf{u}, \mathbf{v}) = \frac{\mathbf{u}^\top \mathbf{v}}{\|\mathbf{u}\|_2 \|\mathbf{v}\|_2}.$$

For embedding level perturbations, $\Delta \in \mathbb{R}^{L \times d_e}$ denotes a continuous perturbation added to $E(x)$, and ∇_Δ denotes the gradient with respect to Δ . Analysis of discrete recovery from continuous perturbations is provided in Appendix B.

3.2 Intra-Task Local Smoothing (Intra-Smooth)

Intra-Smooth promotes local smoothing by training on worst-case embedding perturbations via an inner-outer procedure, where the inner step approximates Δ^* under budget $\varepsilon_{\text{intra}}$, and the outer step updates trainable parameters θ on perturbed samples. From the current batch \mathcal{B} , we sample a subset $\mathcal{B}_{\text{intra}}$. For any $(x, y) \in \mathcal{B}_{\text{intra}}$, the inner perturbation is:

$$\Delta_{\text{intra}}^*(x) = \underset{\|\Delta\|_2 \leq \varepsilon_{\text{intra}}}{\text{argmax}} \mathcal{L}_{\text{sup}}(f_\theta(E(x) + \Delta), y), \quad (1)$$

where \mathcal{L}_{sup} denotes supervised cross entropy loss. The inner maximization seeks an adversarial perturbation within the budget that maximizes the loss. We approximate Equation 1 with K_{intra} steps of PGD (Madry et al., 2018). Let $\Delta^{(0)} = 0$ and iteratively update $\Delta^{(k)}$ by:

$$\Delta^{(k)} = \Pi_{\varepsilon_{\text{intra}}}(\Delta^{(k-1)} + \alpha_{\text{intra}} \cdot \text{Norm}(\nabla_\Delta \mathcal{L}_{\text{sup}}(f_\theta(E(x) + \Delta^{(k-1)}), y))), \quad (2)$$

where $\alpha_{\text{intra}} = \varepsilon_{\text{intra}}/K_{\text{intra}}$, $\text{Norm}(\cdot)$ is ℓ_2 normalization, and Π_ε projects onto the ℓ_2 ball.

The outer adversarial loss is:

$$\mathcal{L}_{\text{intra}} = \mathbb{E}[\mathcal{L}_{\text{sup}}(f_\theta(E(x) + \Delta_{\text{intra}}^*(x)), y)]. \quad (3)$$

Beyond the PGD-based solver, we also consider alternative inner solvers for generating $\Delta_{\text{intra}}^*(x)$.

FGSM computes a single update at $\Delta = 0$ (Goodfellow et al., 2015):

$$\Delta_{\text{intra}}^*(x) = \varepsilon_{\text{intra}} \cdot \text{sign}\left(\nabla_{\Delta} \mathcal{L}_{\text{sup}}(f_{\theta}(E(x) + \Delta), y)\right)\Big|_{\Delta=0}, \quad (4)$$

where $\text{sign}(\cdot)$ denotes element-wise sign function. Unlike Equation 2, FGSM uses an ℓ_{∞} budget, applies one update, and does not involve projection.

Rand samples a random direction and scales it to ℓ_2 budget:

$$\Delta_{\text{intra}}^*(x) = \varepsilon_{\text{intra}} \cdot \frac{\xi}{\|\xi\|_2}, \quad \xi \sim \mathcal{N}(0, I). \quad (5)$$

TRADES replaces supervised loss with a KL consistency objective (Zhang et al., 2019). The inner perturbation is:

$$\Delta_{\text{intra}}^*(x) = \underset{\|\Delta\|_2 \leq \varepsilon_{\text{intra}}}{\text{argmax}} \text{KL}(p_{\theta}(\cdot | x) \| p_{\theta}(\cdot | x, \Delta)), \quad (6)$$

and the outer loss is:

$$\mathcal{L}_{\text{intra}}^{\text{TR}} = \mathbb{E}[\text{KL}(p_{\theta}(\cdot | x) \| p_{\theta}(\cdot | x, \Delta_{\text{intra}}^*(x)))] \quad (7)$$

3.3 Similarity Clipping (Proto-Clip)

Proto-Clip discourages the model from overly strong alignment to the current task prototype $c_t \in \mathbb{R}^d$ via a similarity clipping loss. For the current batch \mathcal{B} , mean representation is:

$$\bar{h} = \frac{1}{|\mathcal{B}|} \sum_x h_{\theta}(x), \quad x \in \mathcal{B}. \quad (8)$$

The prototype is updated by an exponential moving average:

$$c_t \leftarrow m c_t + (1 - m) \bar{h}, \quad (9)$$

where $m \in (0, 1)$ is the momentum coefficient.

Based on c_t , we introduce a penalty that enforces an upper bound on similarity:

$$\mathcal{L}_{\text{clip}} = \mathbb{E}[\max(0, S(h_{\theta}(x), c_t) - \tau_{\text{hi}})]^2, \quad (10)$$

where τ_{hi} is a similarity threshold. This term acts as a soft constraint on overly high similarity and is activated only when $S(h_{\theta}(x), c_t) > \tau_{\text{hi}}$.

3.4 Inter-Task Directional Alignment (Inter-Align)

Inter-Align enhances retention and stability by shrinking the geometric gap between adjacent tasks. We treat the previous task prototype c_{t-1} as a semantic anchor and load it at the start of task t . From the current batch \mathcal{B} , we sample a subset $\mathcal{B}_{\text{inter}}$. For any $x \in \mathcal{B}_{\text{inter}}$, the inner perturbation in embedding space is:

$$\Delta_{\text{inter}}^*(x) = \underset{\|\Delta\|_2 \leq \varepsilon_{\text{inter}}}{\text{argmax}} S(h_{\theta}(E(x) + \Delta), c_{t-1}). \quad (11)$$

This inner maximization seeks the most effective directional alignment perturbation. Maximizing $S(h_{\theta}(E(x) + \Delta), c_{t-1})$ increases alignment to anchor c_{t-1} and narrows local geometric gap to the previous prototype. It is solved in the same manner as Equation 2, but with similarity objective in Equation 11 replacing \mathcal{L}_{sup} , and using $\varepsilon_{\text{inter}}$ and K_{inter} . After obtaining $\Delta_{\text{inter}}^*(x)$, we compute adversarial loss on perturbed embeddings:

$$\mathcal{L}_{\text{inter}} = \mathbb{E}[\mathcal{L}_{\text{sup}}(f_{\theta}(E(x) + \Delta_{\text{inter}}^*(x)), y)]. \quad (12)$$

3.5 Overall Objective

For each batch \mathcal{B} , we sample \mathcal{B}_{std} , $\mathcal{B}_{\text{intra}}$, and $\mathcal{B}_{\text{inter}}$ with fixed ratios. Let \mathcal{L}_{std} denote the standard supervised loss over \mathcal{B}_{std} :

$$\mathcal{L}_{\text{std}} = \mathbb{E}[\mathcal{L}_{\text{sup}}(f_{\theta}(E(x)), y)]. \quad (13)$$

Putting the terms together, the overall objective is:

$$\mathcal{L}(\theta) = \mathcal{L}_{\text{std}} + \lambda_{\text{intra}} \mathcal{L}_{\text{intra}} + \lambda_{\text{clip}} \mathcal{L}_{\text{clip}} + \lambda_{\text{inter}} \mathcal{L}_{\text{inter}}. \quad (14)$$

Except for task prototypes $\{c_t\}$, AdvCL stores neither replay data nor historical models. Adversarial perturbations are generated online during training and are not stored. For robustness evaluation, perturbations are regenerated following evaluation settings.

4 Experimental Setup

4.1 Datasets

We follow Super Natural Instructions (Wang et al., 2022) and construct a CL benchmark with six tasks, spanning both classification and generation: tweet anger detection from SemEval 2018 Task 1 (Mohammad et al., 2018), emotion classification (Saravia et al., 2018), news topic classification on AG

News (Zhang et al., 2015), adversarial natural language inference on ANLI (Nie et al., 2020), extreme summarization on XSum (Narayan et al., 2018), and title generation on XL-Sum (Hasan et al., 2021). These tasks exhibit substantial heterogeneity in cross-task similarity, which we characterize in Appendix A.1. The default order is anger → emotion → agnews → anli → xsum → xlsun. For each task, we randomly sample 2,000 samples for training, 200 for validation, and 200 for testing.

4.2 Baselines

All baselines follow the PEFT-CL setting (Coleman et al., 2025). AdvCL comprises three plug-in modules that can be readily integrated into different CL frameworks, so we evaluate on representative CL frameworks that cover replay, regularization, and dynamic architecture methods. Specifically, we include: (1) **Sequence**, which sequentially fine tunes a single PEFT module across tasks without any CL mechanism. (2) **Replay**, which sequentially updates the same PEFT module while replaying a fixed proportion of samples from each previous task at every stage. (3) **EWC** (Kirkpatrick et al., 2017), which adds a quadratic penalty weighted by parameter importance to constrain PEFT parameters that are critical to past tasks. (4) **MoE**, inspired by prior work (Shazeer et al., 2017; Araujo et al., 2024), which maintains multiple PEFT experts and uses a router to combine experts for each input during sequential training. (5) **Joint**, which trains a single PEFT module on the union of all task data. (6) **Separate**, which trains an independent PEFT module for each task and evaluates by selecting the corresponding module using the given task identity.

4.3 Metrics

We report five CL metrics. **Average Performance (AP)** averages final performance over all tasks after learning the full sequence, using accuracy for classification tasks and ROUGE-L for generation tasks. **Forgetting (FGT)** quantifies drop on each earlier task from its best achieved value during training to its final value. **Forward Transfer (FWT)** evaluates how previously learned knowledge helps future tasks. We report two variants: **FWT-1** uses base model as a zero-shot reference for each upcoming task, while **FWT-2** uses a single-task trained PEFT model as reference. **Backward Transfer (BWT)** measures how learning later tasks affects earlier tasks by comparing final performance to performance right after each

task is learned. Detailed definitions are provided in Appendix A.3.

4.4 Training Settings

All experiments run on a single NVIDIA A100 40GB GPU. We use Llama 3.2 3B Instruct as the backbone and adopt LoRA (Hu et al., 2022) as the PEFT module.

For classification tasks, micro batch size is 16 with gradient accumulation of 8, yielding an effective batch size of 128. For generation tasks, micro batch size is 4 with gradient accumulation of 32. Learning rate is set to $3e-5$ with a warmup ratio of 0.05 and weight decay 0.1. Baseline-specific settings and hyperparameters of three modules are provided in Appendix A.4.

5 Main Results

This section evaluates standard performance across baselines and their module-augmented variants. We present results on module ablation and cross-baseline transferability under the standard setting, as shown in Table 1, where S + C + A denotes AdvCL. Within each model family, the best and second-best results are highlighted in bold and underlined, respectively.

5.1 Module Ablation

See Part I of Table 1 for results. Intra-Smooth trains the model along locally challenging directions in embedding space and serves as a major contributor to overall performance gains. Inter-Align explicitly aligns representations across tasks, which reduces representation drift and improves retention, as reflected by lower forgetting and higher BWT, while its effect on forward transfer is more limited. Proto-Clip alone offers relatively limited gains, but when combined with Intra-Smooth, it strengthens retention-related performance, especially BWT. Intra-Smooth plus Inter-Align is more effective at reducing forgetting and improving FWT-1. Combining all three modules achieves the best results on four metrics, indicating a better trade-off among accuracy, transfer, and forgetting. Additional order results are provided in Appendix C.

In summary, **the three-module combination is the most stable, and two-module combinations generally outperform single-module ones**, reflecting clear complementarity among the modules. The main exception is Proto-Clip plus Inter-Align, where both mechanisms impose additional

Table 1: Results of module ablation and transferability under standard setting.

Model	AP(\uparrow)	FGT(\downarrow)	FWT-1(\uparrow)	FWT-2(\uparrow)	BWT(\uparrow)
Part I: Module Ablation					
Sequence	55.21	3.42	1.65	1.76	-2.11
+ S (Smooth)	55.90	2.70	<u>2.70</u>	1.57	-1.05
+ C (Clip)	55.29	3.38	-0.42	<u>1.99</u>	-2.28
+ A (Align)	55.36	2.20	0.28	1.23	-1.29
+ S + C	<u>55.97</u>	2.30	2.52	1.10	<u>-0.41</u>
+ S + A	55.71	<u>1.80</u>	3.55	1.06	-0.66
+ C + A	54.98	1.95	2.11	0.48	-0.85
+ S + C + A	56.64	1.50	2.38	2.73	0.38
Part II: Transferability					
Replay	55.61	1.70	<u>0.35</u>	0.46	<u>-0.07</u>
+ S (Smooth)	57.89	1.30	3.72	2.99	-0.37
+ C (Clip)	<u>56.09</u>	<u>1.33</u>	-0.54	0.74	0.17
+ A (Align)	55.85	2.00	-1.46	<u>1.47</u>	-1.00
EWC	55.42	3.51	-0.06	1.97	-2.11
+ S (Smooth)	<u>55.66</u>	3.40	3.05	<u>1.76</u>	-1.57
+ C (Clip)	55.61	<u>2.56</u>	<u>0.83</u>	1.28	<u>-1.06</u>
+ A (Align)	55.86	1.80	-0.08	1.08	-0.52
MoE	53.42	4.80	0.46	0.93	-3.27
+ S (Smooth)	54.26	3.30	-1.31	0.86	-2.16
+ C (Clip)	53.84	<u>4.20</u>	<u>0.21</u>	<u>1.26</u>	-3.15
+ A (Align)	<u>54.12</u>	4.40	-0.21	1.38	<u>-2.97</u>
Joint	52.92	-	-	-	-
+ S (Smooth)	56.27	-	-	-	-
Separate	55.20	-	-	-	-
+ S (Smooth)	56.76	-	-	-	-

constraints on optimization and may therefore limit the attainable gains.

5.2 Transferability

See Part II of Table 1 for results. To isolate transferability, we add each module individually to each baseline. All three modules exhibit strong transferability, without any performance collapse, and they typically improve performance. In particular, Intra-Smooth is the most consistently beneficial module across baselines.

Proto-Clip and Inter-Align primarily influence stability, but with different patterns. Proto-Clip penalizes over-alignment to the current prototype and is most effective when paired with other modules. Inter-Align more directly shrinks cross-task representational gaps and shows more consistent

retention benefits, typically reflected in lower forgetting and higher BWT.

Since all unaugmented baselines share the same backbone and training steps, the aggregate metric AP varies only slightly. In contrast, CL metrics show clearer separation. For example, Replay exhibits substantially lower forgetting. Joint tends to achieve lower AP, which may reflect optimization difficulties caused by multi-task objective conflicts or distributional mismatch. Overall, **the modules are plug-and-play and do not depend on specific CL details across training paradigms.**

6 Further Analysis

6.1 Robustness Evaluation

We further conduct cross-attack evaluation under five attacks (PGD-5, PGD-10, FGSM, Rand, and

Table 2: Cross-attack results averaged over five attacks.

Model	AP(\uparrow)	FGT(\downarrow)	FWT-1(\uparrow)	FWT-2(\uparrow)	BWT(\uparrow)
Sequence	37.47	8.78	2.20	1.61	-7.52
+ S (Smooth)	43.23	4.04	3.72	2.50	-1.68
+ C (Clip)	36.24	9.76	1.59	0.67	-7.87
+ A (Align)	39.33	5.14	1.67	-0.38	-3.46
+ S + C + A	44.22	2.76	3.48	2.90	-0.40

discrete perturbations), with averaged results reported in Table 2. Intra-Smooth yields consistent robustness gains, indicating strong generalization. Inter-Align primarily improves stability metrics, especially FGT and BWT. Proto-Clip alone degrades robustness under this evaluation, suggesting an overly restrictive constraint. In contrast, combining all three modules achieves best performance on all metrics, highlighting clear synergistic effects. Additional baselines are provided in Appendix D.1. Robustness under PGD with varying perturbation strengths is also reported in Appendix D.2 and shows a similar overall pattern.

6.2 Intra-Smooth Sensitivity

6.2.1 Perturbation Strength.

Part I of Table 3 shows the effect of different perturbation strengths in Intra-Smooth. FGT and BWT vary non-monotonically with $\varepsilon_{\text{intra}}$. Small perturbations (0.05, 0.10) behave like a mild regularizer for local smoothing, reducing forgetting and improving BWT. Intermediate strengths (0.15, 0.20) form a transition region, where perturbations amplify conflicts with stability on clean samples, but do not yield a sufficiently consistent smoothing signal. As a result, stability degrades and AP drops. With larger perturbations (0.25, 0.30), adversarial examples become consistently harder across samples, which strengthens the smoothing effect and restores stability, with AP recovering accordingly.

In contrast, FWT decreases as $\varepsilon_{\text{intra}}$ grows, suggesting that stronger smoothing constrains effective updates and favors neighborhood consistency over forward transfer.

6.2.2 Perturbation Solver.

Part II of Table 3 compares different perturbation solvers. Within PGD- K family, increasing K reveals a clear trade-off between stability and plasticity. Larger K tends to raise FWT, while retention metrics can degrade, with higher forgetting and a more negative BWT. Compared with PGD-1, al-

ternative solvers do not offer a consistent improvement across metrics. PGD-1 All perturbs both instruction and input tokens, which often hurts stability. Rand lacks worst-case optimization and therefore offers little benefit. TRADES-1 and FGSM achieve AP comparable to PGD-1, but their retention metrics are less reliable than it. TRADES-1 optimizes a different objective, while FGSM follows a different perturbation constraint. Empirically, PGD-1 is a reliable and well-balanced default choice across metrics.

6.3 Inter-Align Geometry

To examine how Inter-Align affects representation geometry across tasks, we quantify geometric relationship between adjacent tasks in representation space using three complementary metrics: (1) **Centroid Cosine Distance** measures global gap between representation centroids of previous and current tasks; (2) **Mean Pairwise Cosine Distance** measures distributional gap by averaging cosine distances over cross-task sample pairs; and (3) **Directional Prototype Alignment** measures alignment strength between current task representations and previous task prototype direction. Using representations extracted after training each task, Inter-Align yields average changes of -4.35%, -0.61%, and +0.33% on these three metrics, respectively, compared with sequence training over adjacent task pairs. These results suggest that Inter-Align narrows cross-task geometric gaps and strengthens directional alignment. See Appendix E for detailed metric definitions and results.

Further analysis of similarity shift under directional perturbations, together with the impact of $\varepsilon_{\text{inter}}$ on continual learning metrics, is provided in Appendix F.

6.4 Computational Overhead Analysis

To quantify computational cost of each module, we compare their additional training overhead under default settings. Intra-Smooth and Inter-

Table 3: Standard evaluation on Sequence baseline with Intra-Smooth. Left: sensitivity to perturbation strength $\varepsilon_{\text{intra}}$. Right: comparison of different solvers used to generate adversarial perturbations. FWT is computed by averaging FWT-1 and FWT-2. Finer-grained $\varepsilon_{\text{intra}}$ values show the same trend and are omitted for brevity. The suffix “- K ” indicates using K_{intra} steps to generate perturbations, and “All” means perturbing both instruction and input embeddings.

Part I: Perturbation Strength ($\varepsilon_{\text{intra}}$)					Part II: Perturbation Solver				
Setting	AP (\uparrow)	FGT (\downarrow)	FWT (\uparrow)	BWT (\uparrow)	Setting	AP (\uparrow)	FGT (\downarrow)	FWT (\uparrow)	BWT (\uparrow)
0.00	55.21	3.42	1.71	-2.11	PGD-1	55.90	2.70	2.14	-1.05
0.05	55.75	2.70	2.16	-1.59	PGD-3	55.81	3.56	3.17	-3.16
0.10	55.90	2.70	2.14	-1.05	PGD-10	55.94	3.93	3.26	-3.53
0.15	53.87	6.04	2.55	-4.94	TRADES-1	55.78	3.17	1.41	-1.97
0.20	54.78	4.90	0.90	-3.25	FGSM	56.30	3.03	2.00	-1.53
0.25	55.70	3.06	0.49	-1.56	Rand	55.14	3.38	0.58	-1.78
0.30	56.66	1.55	0.22	-0.05	PGD-1 All	55.05	4.46	2.29	-3.16

Align incur approximately +25% and +12.5% additional computation, respectively. Proto-Clip is computed using activations from baseline training step and thus introduces negligible extra computation. Overall, the computational overhead remains predictable and manageable. Three-module combination adds about +37.5% computation, which is justified given the gains. More details are provided in Appendix G.

6.5 Additional Performance Analysis

We further analyze the proposed method from two perspectives: per-task stagewise behavior and the relationship between standard and robust performance. Detailed results are provided in Appendix H. First, the per-task stagewise performance curves show that the three-module combination mainly supports long-term stability and transfer across stages, rather than maximizing performance at each stage. Although the gains differ across tasks, it generally leads to more stable trajectories and better preservation of earlier-task performance in later stages.

Second, we compare standard and robust average performance under two PGD-based evaluation settings. Results suggest that standard and robust performance do not follow a simple trade-off. In most cases, adding our modules improves robustness while maintaining competitive or better standard performance. Intra-Smooth provides the most consistent gains, while the full combination remains strong overall.

7 Conclusion

We propose AdvCL, which repurposes adversarial perturbations as a geometric control signal for CL. AdvCL includes three transferable plug-in modules, Intra-Smooth promotes local smoothing and robustness, Proto-Clip prevents over-alignment to current prototype, and Inter-Align reduces cross-task representational gaps via directional alignment. Experiments show consistent gains in both standard performance and robustness, with reduced forgetting and better transfer.

References

- Alessandro Achille, Michael Lam, Rahul Tewari, Avinash Ravichandran, Subhansu Maji, Charless C. Fowlkes, Stefano Soatto, and Pietro Perona. 2019. Task2vec: Task embedding for meta-learning. In *Proceedings of the IEEE/CVF International Conference on Computer Vision (ICCV)*.
- Armen Aghajanyan, Akshat Shrivastava, Ankit Gupta, Naman Goyal, Luke Zettlemoyer, and Sonal Gupta. 2021. Better fine-tuning by reducing representational collapse. In *International Conference on Learning Representations*.
- Vladimir Araujo, Marie-Francine Moens, and Tinne Tuytelaars. 2024. Learning to route for dynamic adapter composition in continual learning with language models. In *Findings of the Association for Computational Linguistics: EMNLP 2024*, pages 687–696, Miami, Florida, USA. Association for Computational Linguistics.
- Samuel J. Bell and Neil D. Lawrence. 2022. The effect of task ordering in continual learning. *Preprint*, arXiv:2205.13323.

- Hyuntak Cha, Jaeho Lee, and Jinwoo Shin. 2021. Co2l: Contrastive continual learning. In *Proceedings of the IEEE/CVF International Conference on Computer Vision (ICCV)*, pages 9516–9525.
- Eric Nuertey Coleman, Luigi Quarantiello, Ziyue Liu, Qinwen Yang, Samrat Mukherjee, Julio Hurtado, and Vincenzo Lomonaco. 2025. [Parameter-efficient continual fine-tuning: A survey](#). Preprint, arXiv:2504.13822.
- Li Cui, Deqing Yang, Jiaxin Yu, Chengwei Hu, Jiayang Cheng, Jingjie Yi, and Yanghua Xiao. 2021. [Refining sample embeddings with relation prototypes to enhance continual relation extraction](#). In *Proceedings of the 59th Annual Meeting of the Association for Computational Linguistics and the 11th International Joint Conference on Natural Language Processing (Volume 1: Long Papers)*, pages 232–243, Online. Association for Computational Linguistics.
- Pierre Foret, Ariel Kleiner, Hossein Mobahi, and Behnam Neyshabur. 2021. Sharpness-aware minimization for efficiently improving generalization. In *International Conference on Learning Representations*.
- Ian J. Goodfellow, Jonathon Shlens, and Christian Szegedy. 2015. Explaining and harnessing adversarial examples. In *International Conference on Learning Representations*.
- Jiayi Han, Liang Du, Hongwei Du, Xiangguo Zhou, Yiwen Wu, Yuanfang Zhang, Weibo Zheng, and Donghong Han. 2025. [SLIM: Let LLM learn more and forget less with soft LoRA and identity mixture](#). In *Proceedings of the 2025 Conference of the Nations of the Americas Chapter of the Association for Computational Linguistics: Human Language Technologies (Volume 1: Long Papers)*, pages 4792–4804, Albuquerque, New Mexico. Association for Computational Linguistics.
- Tahmid Hasan, Abhik Bhattacharjee, Md. Saiful Islam, Kazi Mubasshir, Yuan-Fang Li, Yong-Bin Kang, M. Sohel Rahman, and Rifat Shahriyar. 2021. [XL-sum: Large-scale multilingual abstractive summarization for 44 languages](#). In *Findings of the Association for Computational Linguistics: ACL-IJCNLP 2021*, pages 4693–4703, Online. Association for Computational Linguistics.
- Naoki Hiratani. 2024. [Disentangling and mitigating the impact of task similarity for continual learning](#). In *Advances in Neural Information Processing Systems*, volume 37, pages 3243–3274. Curran Associates, Inc.
- Neil Houlsby, Andrei Giurgiu, Stanislaw Jastrzebski, Bruna Morrone, Quentin De Laroussilhe, Andrea Gesmundo, Mona Attariyan, and Sylvain Gelly. 2019. Parameter-efficient transfer learning for NLP. In *Proceedings of the 36th International Conference on Machine Learning*, volume 97 of *Proceedings of Machine Learning Research*, pages 2790–2799. PMLR.
- Edward J Hu, Yelong Shen, Phillip Wallis, Zeyuan Allen-Zhu, Yuanzhi Li, Shean Wang, Lu Wang, and Weizhu Chen. 2022. LoRA: Low-rank adaptation of large language models. In *International Conference on Learning Representations*.
- Jianheng Huang, Leyang Cui, Ante Wang, Chengyi Yang, Xinting Liao, Linfeng Song, Junfeng Yao, and Jinsong Su. 2024. [Mitigating catastrophic forgetting in large language models with self-synthesized rehearsal](#). In *Proceedings of the 62nd Annual Meeting of the Association for Computational Linguistics (Volume 1: Long Papers)*, pages 1416–1428, Bangkok, Thailand. Association for Computational Linguistics.
- Neel Jain, Ping-yeh Chiang, Yuxin Wen, John Kirchenbauer, Hong-Min Chu, Gowthami Somepalli, Brian R. Bartoldson, Bhavya Kailkhura, Avi Schwarzschild, Aniruddha Saha, Micah Goldblum, Jonas Geiping, and Tom Goldstein. 2024. NEFTune: Noisy embeddings improve instruction finetuning. In *The Twelfth International Conference on Learning Representations*.
- Jiaming Ji, Kaile Wang, Tianyi Alex Qiu, Boyuan Chen, Jiayi Zhou, Changye Li, Hantao Lou, Josef Dai, Yunhuai Liu, and Yaodong Yang. 2025. [Language models resist alignment: Evidence from data compression](#). In *Proceedings of the 63rd Annual Meeting of the Association for Computational Linguistics (Volume 1: Long Papers)*, pages 23411–23432, Vienna, Austria. Association for Computational Linguistics.
- Haoming Jiang, Pengcheng He, Weizhu Chen, Xiaodong Liu, Jianfeng Gao, and Tuo Zhao. 2020. [SMART: Robust and efficient fine-tuning for pre-trained natural language models through principled regularized optimization](#). In *Proceedings of the 58th Annual Meeting of the Association for Computational Linguistics*, pages 2177–2190, Online. Association for Computational Linguistics.
- Nitish Shirish Keskar, Dheevatsa Mudigere, Jorge Nocedal, Mikhail Smelyanskiy, and Ping Tak Peter Tang. 2017. On large-batch training for deep learning: Generalization gap and sharp minima. In *International Conference on Learning Representations*.
- James Kirkpatrick, Razvan Pascanu, Neil Rabinowitz, Joel Veness, Guillaume Desjardins, Andrei A. Rusu, Kieran Milan, John Quan, Tiago Ramalho, Agnieszka Grabska-Barwinska, Demis Hassabis, Claudia Clopath, Dharshan Kumaran, and Raia Hadsell. 2017. [Overcoming catastrophic forgetting in neural networks](#). *Proceedings of the National Academy of Sciences*, 114(13):3521–3526.
- Brian Lester, Rami Al-Rfou, and Noah Constant. 2021. [The power of scale for parameter-efficient prompt tuning](#). In *Proceedings of the 2021 Conference on Empirical Methods in Natural Language Processing*, pages 3045–3059, Online and Punta Cana, Dominican Republic. Association for Computational Linguistics.

- Yuheng Lu, Bingshuo Qian, Caixia Yuan, Huixing Jiang, and Xiaojie Wang. 2025. [Controlled low-rank adaptation with subspace regularization for continued training on large language models](#). In *Proceedings of the 63rd Annual Meeting of the Association for Computational Linguistics (Volume 1: Long Papers)*, pages 19165–19181, Vienna, Austria. Association for Computational Linguistics.
- Aleksander Madry, Aleksandar Makelov, Ludwig Schmidt, Dimitris Tsipras, and Adrian Vladu. 2018. Towards deep learning models resistant to adversarial attacks. In *International Conference on Learning Representations*.
- Takeru Miyato, Shin-Ichi Maeda, Masanori Koyama, and Shin Ishii. 2019. [Virtual adversarial training: A regularization method for supervised and semi-supervised learning](#). *IEEE Transactions on Pattern Analysis and Machine Intelligence*, 41(8):1979–1993.
- Saif Mohammad, Felipe Bravo-Marquez, Mohammad Salameh, and Svetlana Kiritchenko. 2018. [SemEval-2018 task 1: Affect in tweets](#). In *Proceedings of the 12th International Workshop on Semantic Evaluation*, pages 1–17, New Orleans, Louisiana. Association for Computational Linguistics.
- Shashi Narayan, Shay B. Cohen, and Mirella Lapata. 2018. [Don’t give me the details, just the summary! topic-aware convolutional neural networks for extreme summarization](#). In *Proceedings of the 2018 Conference on Empirical Methods in Natural Language Processing*, pages 1797–1807, Brussels, Belgium. Association for Computational Linguistics.
- Yixin Nie, Adina Williams, Emily Dinan, Mohit Bansal, Jason Weston, and Douwe Kiela. 2020. [Adversarial NLI: A new benchmark for natural language understanding](#). In *Proceedings of the 58th Annual Meeting of the Association for Computational Linguistics*, pages 4885–4901, Online. Association for Computational Linguistics.
- Sylvestre-Alvise Rebuffi, Alexander Kolesnikov, Georg Sperl, and Christoph H. Lampert. 2017. [icarl: Incremental classifier and representation learning](#). In *Proceedings of the IEEE Conference on Computer Vision and Pattern Recognition (CVPR)*.
- Xiaolei Ru, Xiaowei Cao, Zijia Liu, Jack Murdoch Moore, Xin-Ya Zhang, Xia Zhu, Wenjia Wei, and Gang Yan. 2024. [Maintaining adversarial robustness in continuous learning](#). *Preprint*, arXiv:2402.11196.
- Andrei A. Rusu, Neil C. Rabinowitz, Guillaume Desjardins, Hubert Soyer, James Kirkpatrick, Koray Kavukcuoglu, Razvan Pascanu, and Raia Hadsell. 2016. [Progressive neural networks](#). *Preprint*, arXiv:1606.04671.
- Elvis Saravia, Hsien-Chi Toby Liu, Yen-Hao Huang, Junlin Wu, and Yi-Shin Chen. 2018. [CARER: Contextualized affect representations for emotion recognition](#). In *Proceedings of the 2018 Conference on Empirical Methods in Natural Language Processing*, pages 3687–3697, Brussels, Belgium. Association for Computational Linguistics.
- Noam Shazeer, Azalia Mirhoseini, Krzysztof Maziarz, Andy Davis, Quoc Le, Geoffrey Hinton, and Jeff Dean. 2017. [Outrageously large neural networks: The sparsely-gated mixture-of-experts layer](#). In *International Conference on Learning Representations*.
- Hong Wang, Wenhan Xiong, Mo Yu, Xiaoxiao Guo, Shiyu Chang, and William Yang Wang. 2019. [Sentence embedding alignment for lifelong relation extraction](#). In *Proceedings of the 2019 Conference of the North American Chapter of the Association for Computational Linguistics: Human Language Technologies, Volume 1 (Long and Short Papers)*, pages 796–806, Minneapolis, Minnesota. Association for Computational Linguistics.
- Mingyang Wang, Heike Adel, Lukas Lange, Jannik Strötgen, and Hinrich Schuetze. 2024. [Rehearsal-free modular and compositional continual learning for language models](#). In *Proceedings of the 2024 Conference of the North American Chapter of the Association for Computational Linguistics: Human Language Technologies (Volume 2: Short Papers)*, pages 469–480, Mexico City, Mexico. Association for Computational Linguistics.
- Xiao Wang, Tianze Chen, Qiming Ge, Han Xia, Rong Bao, Rui Zheng, Qi Zhang, Tao Gui, and Xuanjing Huang. 2023. [Orthogonal subspace learning for language model continual learning](#). In *Findings of the Association for Computational Linguistics: EMNLP 2023*, pages 10658–10671, Singapore. Association for Computational Linguistics.
- Yizhong Wang, Swaroop Mishra, Pegah Alipoormolabashi, Yeganeh Kordi, Amirreza Mirzaei, Atharva Naik, Arjun Ashok, Arut Selvan Dhanasekaran, Anjana Arunkumar, David Stap, Eshaan Pathak, Gianis Karamanolakis, Haizhi Lai, Ishan Purohit, Ishani Mondal, Jacob Anderson, Kirby Kuznia, Krima Doshi, Kuntal Kumar Pal, and 16 others. 2022. [Super-NaturalInstructions: Generalization via declarative instructions on 1600+ NLP tasks](#). In *Proceedings of the 2022 Conference on Empirical Methods in Natural Language Processing*, pages 5085–5109, Abu Dhabi, United Arab Emirates. Association for Computational Linguistics.
- Zhenyi Wang and Heng Huang. 2024. [Model sensitivity aware continual learning](#). In *Advances in Neural Information Processing Systems*, volume 37, pages 132583–132613. Curran Associates, Inc.
- Hongyang Zhang, Yaodong Yu, Jiantao Jiao, Eric Xing, Laurent El Ghaoui, and Michael Jordan. 2019. [Theoretically principled trade-off between robustness and accuracy](#). In *Proceedings of the 36th International Conference on Machine Learning*, volume 97 of *Proceedings of Machine Learning Research*, pages 7472–7482. PMLR.

- Xiang Zhang, Junbo Zhao, and Yann LeCun. 2015. Character-level convolutional networks for text classification. In *Advances in Neural Information Processing Systems*, volume 28. Curran Associates, Inc.
- Kang Zhao, Hua Xu, Jiangong Yang, and Kai Gao. 2022. Consistent representation learning for continual relation extraction. In *Findings of the Association for Computational Linguistics: ACL 2022*, pages 3402–3411, Dublin, Ireland. Association for Computational Linguistics.
- Weixiang Zhao, Shilong Wang, Yulin Hu, Yanyan Zhao, Bing Qin, Xuanyu Zhang, Qing Yang, Dongliang Xu, and Wanxiang Che. 2024. SAPT: A shared attention framework for parameter-efficient continual learning of large language models. In *Proceedings of the 62nd Annual Meeting of the Association for Computational Linguistics (Volume 1: Long Papers)*, pages 11641–11661, Bangkok, Thailand. Association for Computational Linguistics.
- Chen Zhu, Yu Cheng, Zhe Gan, Siqi Sun, Tom Goldstein, and Jingjing Liu. 2020. FreeLB: Enhanced adversarial training for natural language understanding. In *International Conference on Learning Representations*.

A Experimental Details

A.1 Dataset Details

Tweet Anger Detection (anger). A binary classification task for affect detection on social media. Given a tweet, the model predicts whether the tweet expresses anger. The dataset comes from SemEval 2018 Task 1 (Mohammad et al., 2018). *Instruction: You are given a tweet. Decide if it expresses anger. Use the following numeric labels: 0 = Not angry; 1 = Angry.*

Emotion Classification (emotion). A multi-class classification task for recognizing the emotion expressed in a sentence. Given a sentence, the model predicts one emotion label. The dataset comes from (Saravia et al., 2018). *Instruction: You are given a tweet. Identify the emotion it expresses. Use the following numeric labels: 0 = anger; 1 = fear; 2 = joy; 3 = love; 4 = sadness; 5 = surprise.*

News Topic Classification (agnews). A news topic classification task. Given a short news article, the model predicts its topic. The dataset comes from AG News (Zhang et al., 2015). *Instruction: You are given a news article. Classify its topic. Use the following numeric labels: 0 = World; 1 = Sports; 2 = Business; 3 = Science/Technology.*

Adversarial Natural Language Inference (anli). A natural language inference task. Each example consists of a premise and a hypothesis, and the model predicts whether the hypothesis entails, contradicts, or is neutral with respect to the premise. The dataset comes from ANLI (Nie et al., 2020). *Instruction: You are given a premise and a hypothesis. Determine their logical relation. Use the following numeric labels: 0 = Contradiction; 1 = Neutral; 2 = Entailment.*

Extreme Summarization (xsum). A conditional generation task. Given a news article, the model generates a single-sentence summary that captures the core point of the article. The dataset comes from XSum (Narayan et al., 2018). *Instruction: You are given a news article. Write a one-sentence summary.*

Title Generation (xsum). A conditional generation task. Given a news text, the model generates a concise title. The dataset comes from XL-Sum (Hasan et al., 2021). *Instruction: You are given a news article. Generate a concise headline.*

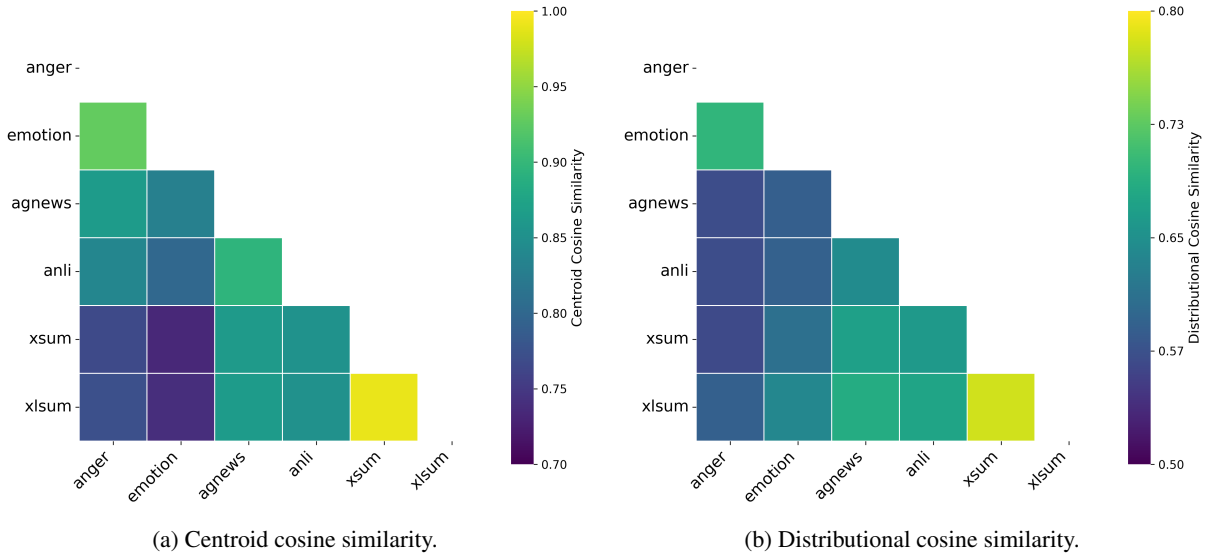


Figure 3: Cross-task similarity in representation space.

All datasets are in English. Beyond individual task details, we characterize similarity across tasks in representation space. Specifically, we compute cosine similarity at both centroid and distributional levels based on representations from a fixed encoder. As shown in Figure 3, the benchmark exhibits substantial heterogeneity in cross-task similarity, xsum and xlsun are highly similar, anger and emotion show moderate similarity, while most other task pairs are well separated. Notably, we do not compute any predefined task similarity before the task sequence, nor use it to make any task-level decisions beyond the current stage. At each stage, only the current task data and the previous task prototype are available.

A.2 Baseline Details

Sequence. Sequence is the simplest CL baseline. A single PEFT module is trained sequentially, using only the current task’s data at each stage, following the predefined task order. After finishing task t , the same PEFT parameters are reused as initialization for task $t+1$, without any explicit anti-forgetting mechanism.

Replay. Replay augments sequential training with a memory buffer that stores samples from previous tasks. At each stage, training batches are formed by mixing current data with replay samples. The PEFT module is still a single adapter updated sequentially, but replay provides a direct rehearsal signal that helps retain past knowledge. The buffer is updated after each stage by adding samples from the current task.

EWC. EWC adds a quadratic penalty that discourages changing parameters deemed important for previous tasks during training on a new task (Kirkpatrick et al., 2017). In our PEFT setting, the EWC penalty is applied only to trainable PEFT parameters, while the backbone remains frozen.

Concretely, after finishing task t , we estimate a diagonal Fisher approximation $F_{t,i}$ for each trainable PEFT parameter θ_i based on squared loss gradients on task t . Let θ_s^* denote the learned parameter vector after task s , and $\theta_{s,i}^*$ its i -th entry. We adopt an online accumulated variant that maintains:

$$P_i = \sum_{s \leq t} F_{s,i}, \quad \mu_i = \frac{\sum_{s \leq t} F_{s,i} \theta_{s,i}^*}{P_i}. \quad (15)$$

When learning task $t+1$, EWC adds a quadratic penalty:

$$\mathcal{L}_{\text{EWC}}(\theta) = \frac{\lambda_{\text{EWC}}}{2} \sum_i P_i (\theta_i - \mu_i)^2, \quad (16)$$

which discourages changing parameters that are important for previously learned tasks.

MoE. Our MoE baseline maintains multiple PEFT experts and uses a learned router to softly combine experts for each input during sequential training. Instead of a single PEFT module, each target module is equipped with N_e PEFT experts, where expert e provides a parameterized update $\Delta_e(\cdot)$. Let x denote the layer input and W_{base} the frozen backbone weight. The MoE layer output is:

$$y = xW_{\text{base}} + \sum_{e=1}^{N_e} \pi_e(x) \Delta_e(x), \quad (17)$$

where $\pi(x) \in \mathbb{R}^E$ is the routing distribution produced by a shared router.

In our implementation, a shared router computes the routing distribution $\pi(x)$ from a pooled layer input. Specifically, it first averages token representations into a single vector, then feeds it into a lightweight two-layer MLP with a softmax output. During training, we freeze the backbone and update only the router and the PEFT expert parameters.

Joint. Joint trains a single PEFT module on the union of data from all tasks. It does not follow the continual learning constraint because it assumes that all task data are available for training.

Separate. Separate trains an independent PEFT module for each task, without parameter sharing across tasks. At evaluation time, it selects the corresponding task-specific module using the given task identity.

A.3 Metric Details

Let T be number of tasks in a sequence. Let $a_{i,j}$ denote performance on test set of task j after completing training on task i , where $i \in \{1, \dots, T\}$ and $j \in \{1, \dots, T\}$. For classification tasks, $a_{i,j}$ is accuracy, and for generation tasks, $a_{i,j}$ is ROUGE-L. Let $a_{0,j}$ denote performance on task j evaluated at initialization, before any training is performed. Let a_j^{sep} denote performance of a model trained on task j only in a single-task setting.

Average Performance (AP). AP measures overall ability after learning full sequence, computed as mean final performance across tasks:

$$\text{AP} = \frac{1}{T} \sum_{j=1}^T a_{T,j}. \quad (18)$$

Forgetting (FGT). Forgetting quantifies worst-case performance drop on each past task over training. For each task $j \leq T - 1$, define:

$$a_j^{\max} = \max_{i=j, \dots, T} a_{i,j}, \quad (19)$$

$$F_j = a_j^{\max} - a_{T,j}, \quad j = 1, \dots, T - 1, \quad (20)$$

where a_j^{\max} is best performance achieved on task j after it is first learned. Mean forgetting over the first $T - 1$ tasks is:

$$\text{Forgetting} = \frac{1}{T-1} \sum_{j=1}^{T-1} F_j. \quad (21)$$

Forward Transfer (FWT). FWT measures benefit of prior learning on a new task. Two variants are reported.

(1) FWT-1 (zero-shot reference):

$$\text{FWT-1} = \frac{1}{T-1} \sum_{j=2}^T (a_{j-1,j} - a_{0,j}), \quad (22)$$

where $a_{j-1,j}$ evaluates model after task $j - 1$ on task j without training on task j .

(2) FWT-2 (single-task reference):

$$\text{FWT-2} = \frac{1}{T} \sum_{j=1}^T (a_{j,j} - a_j^{\text{sep}}). \quad (23)$$

Backward Transfer (BWT). BWT measures effect of later learning on earlier tasks by comparing final performance on each past task to performance right after learning that task:

$$\text{BWT} = \frac{1}{T-1} \sum_{j=1}^{T-1} (a_{T,j} - a_{j,j}). \quad (24)$$

A.4 Training Details

All experiments run on a single NVIDIA A100 40GB GPU. We use Llama 3.2 3B Instruct¹ as the frozen backbone and adopt LoRA (Hu et al., 2022) as the PEFT module.

For non-MoE baselines, i.e., Sequence, Replay, EWC, Joint, and Separate, LoRA uses rank $r=32$, scaling factor $\alpha=64$, and dropout=0.1. Target modules are q_proj, k_proj, v_proj, o_proj, gate_proj, up_proj, and down_proj. For MoE, we use $N_e=6$ LoRA experts. Each expert uses rank $r=32$, $\alpha=64$, and dropout=0.1, and MoE-LoRA is applied only to q_proj, k_proj, v_proj, and o_proj.

For Replay, after finishing each task, we randomly sample 0.02 of its training samples and store them for replay in subsequent stages.

For Intra-Smooth, we sample a subset $\mathcal{B}_{\text{intra}}$ from each mini-batch with ratio $r_{\text{intra}}=0.25$. We set $\epsilon_{\text{intra}}=0.1$, $k_{\text{intra}}=1$, and $\lambda_{\text{intra}}=0.1$. For Proto-Clip, we use momentum coefficient $m=0.9$ and threshold $\tau_{\text{hi}}=0.8$, with $\lambda_{\text{clip}}=0.5$. For Inter-Align, we sample a subset $\mathcal{B}_{\text{inter}}$ from each mini-batch with ratio $r_{\text{inter}}=0.125$. We set $\epsilon_{\text{inter}}=0.03$, $k_{\text{inter}}=1$, and $\lambda_{\text{inter}}=0.05$.

¹<https://huggingface.co/meta-llama/Llama-3.2-3B-Instruct>

Table 4: Discrete recovery statistics under embedding-level PGD-1 perturbations with $\epsilon=0.1$. All values are multiplied by 100 for readability.

Task	Overall Shift	Per-Token Shift	Token Change Rate	Min Margin
anger	4.72	0.75	0.00	7.78
emotion	3.81	0.67	0.00	13.33
agnews	4.47	0.46	0.00	7.78
anli	4.72	0.30	0.00	7.47
xsum	5.10	0.13	0.00	7.28
xlsum	5.72	0.13	0.00	7.28

For classification tasks, the micro-batch size is 16 with gradient accumulation of 8, yielding an effective batch size of 128. For generation tasks, the micro-batch size is 4 with gradient accumulation of 32. We use a learning rate of $3e-5$ with a warmup ratio of 0.05 and weight decay 0.1.

We set maximum input length to 512 tokens and maximum output length to 64 tokens. For each stage, we train for 160 steps if current task is a classification task, and for 20 steps if it is a generation task.

For generation evaluation, we use beam search with 4 beams, prevent 3-gram repetitions, and set the length penalty to 1.1. All reported results are averaged over three runs with different random seeds.

B Discrete Recovery from Continuous Perturbations

To assess discrete visibility of embedding-level continuous perturbations, we perform a discrete recovery analysis. Given an input token sequence $x = (x_1, \dots, x_L)$, its embedding representation is $E(x) \in \mathbb{R}^{L \times d_e}$. We apply a continuous perturbation $\Delta \in \mathbb{R}^{L \times d_e}$ to obtain the perturbed embeddings $E(x) + \Delta$. To facilitate analysis, we map each perturbed embedding vector $(E(x) + \Delta)_i$ back to a proxy discrete token by nearest-neighbor retrieval in the vocabulary embedding space using cosine similarity. This recovery is used only to characterize how continuous perturbations translate into discrete token changes, and should not be interpreted as explicit discrete substitution attacks.

We report four metrics: (1) **Overall Shift**, $\|\Delta\|_F$ averaged across samples; (2) **Per-token Shift**, $\|\Delta_i\|_2$ averaged across token positions within each sample, and then across samples; (3) **Token Change Rate**, the fraction of token positions where the nearest-neighbor recovered token differs from

the original token, i.e., the proportion of positions whose discrete token changes after recovery; and (4) **Min Margin**, the minimum cosine similarity gap $s_{\text{orig}} - s_{\text{alt}}$, where s_{orig} is the cosine similarity between the perturbed embedding and the original token embedding, and s_{alt} is the highest cosine similarity to any alternative token. Smaller values indicate the recovered discrete token is closer to changing.

Table 4 reports results across all six tasks under PGD-1 with $\epsilon=0.1$. Both Overall Shift and Per-Token Shift are consistently non-zero across tasks, indicating a stable perturbation size in embedding space. In contrast, Token Change Rate is 0 for all tasks and Min margin remains positive, suggesting that nearest-neighbor recovery yields the same discrete tokens as the original input. These observations indicate that embedding-level perturbations can substantially modify continuous representations while leaving the recovered discrete tokens unchanged, which explains why the perturbations are largely imperceptible at the token level.

C Additional Order Results

In addition to default task order, we also evaluate baselines under an alternative order: emotion \rightarrow agnews \rightarrow anger \rightarrow xsum \rightarrow xlsum \rightarrow anli. Results are reported in Table 5. For the alternative task order, we directly reuse the hyperparameters from the default task order without further tuning. Overall, trends are consistent with Table 1, indicating that our modules yields stable improvements across different task orders.

D Robustness Evaluation

D.1 Cross-Attack Evaluation

We evaluate different baselines under five attack settings: PGD-5, PGD-10, FGSM, Rand, and explicit discrete perturbations. For PGD-5, PGD-10,

Table 5: Results of additional task order under Standard and PGD settings. \uparrow indicates higher is better, while \downarrow indicates lower is better. + S, + C, and + A denote augmenting a baseline with Intra-Smooth, Proto-Clip, and Inter-Align, respectively. The best and second-best results are highlighted in **bold** and underlined, respectively.

Model	Standard					PGD (Input)				
	AP (\uparrow)	FGT (\downarrow)	FWT-1 (\uparrow)	FWT-2 (\uparrow)	BWT (\uparrow)	AP (\uparrow)	FGT (\downarrow)	FWT-1 (\uparrow)	FWT-2 (\uparrow)	BWT (\uparrow)
Sequence	53.15	3.70	0.24	0.42	-2.98	32.34	8.47	2.21	-0.04	-7.89
+ S (Smooth)	<u>55.43</u>	<u>2.30</u>	-0.64	1.61	<u>-1.66</u>	<u>39.63</u>	<u>4.60</u>	4.49	4.38	<u>-4.45</u>
+ C (Clip)	54.62	3.41	<u>0.56</u>	2.25	-3.41	30.47	10.69	1.64	-0.42	-9.69
+ A (Align)	53.94	3.97	0.77	1.73	-3.60	30.17	11.07	2.21	-0.73	-9.67
+ S + C + A	56.09	1.63	-0.87	<u>1.80</u>	-1.11	42.12	1.15	<u>2.54</u>	<u>2.96</u>	0.24

and Rand, perturbations are constrained in ℓ_2 norm with budget $\varepsilon=0.1$ in embedding space. For FGSM, perturbations are constrained in ℓ_∞ norm with budget $\varepsilon=5e-4$ in embedding space. For discrete perturbations, we apply TextAttack² to perturb 10% of words for classification tasks and 5% of words for generation tasks via synonym substitutions and typographical perturbations.

The averaged results across five attacks are reported in Table 6. Intra-Smooth is the key contributor to robustness improvements. Inter-Align mainly helps mitigate forgetting and improves BWT. Combining all three modules further strengthens robustness beyond Intra-Smooth alone, achieving the best overall performance across all metrics.

D.2 Robustness under PGD

As shown in Figure 4, robust AP decreases monotonically as perturbation strength ϵ increases. Intra-Smooth yields consistent gains, since its perturbation form is more aligned with PGD evaluation. In contrast, mechanisms of Proto-Clip and Inter-Align are not fully matched to this evaluation setting, yet combining three modules still maintains higher robustness, indicating complementary gains among modules.

E Geometric Metrics for Inter-Align

E.1 Metric Definitions

Let $E(\cdot)$ denote the encoder that maps an input sample to a representation vector. We use ℓ_2 normalized representations $\mathbf{z} = E(x)/\|E(x)\|_2$ and compute cosine similarity and cosine distance accordingly. For each adjacent task pair, we denote the previous task by p and the current task by c . Let $\mathcal{Z}_p = \{\mathbf{z}_i^p\}_{i=1}^{n_p}$ and $\mathcal{Z}_c = \{\mathbf{z}_j^c\}_{j=1}^{n_c}$ be the sets

of normalized representations from previous current tasks, respectively. We use $S(\mathbf{u}, \mathbf{v})$ for cosine similarity and $1 - S(\mathbf{u}, \mathbf{v})$ for cosine distance.

Centroid Cosine Distance. We represent each task by a centroid prototype in representation space. Specifically, we compute the mean representation within each task and then apply ℓ_2 normalization:

$$\bar{\mathbf{z}}_p = \frac{1}{n_p} \sum_{i=1}^{n_p} \mathbf{z}_i^p, \quad \bar{\mathbf{z}}_c = \frac{1}{n_c} \sum_{j=1}^{n_c} \mathbf{z}_j^c, \quad (25)$$

$$\hat{\mathbf{z}}_p = \frac{\bar{\mathbf{z}}_p}{\|\bar{\mathbf{z}}_p\|_2}, \quad \hat{\mathbf{z}}_c = \frac{\bar{\mathbf{z}}_c}{\|\bar{\mathbf{z}}_c\|_2}. \quad (26)$$

Centroid cosine distance is defined as:

$$d_{\text{cent}} = 1 - S(\hat{\mathbf{z}}_p, \hat{\mathbf{z}}_c). \quad (27)$$

This metric captures global gap between the mean representation prototypes of previous and current tasks. A smaller value indicates closer centroids. If this value decreases after adding Inter-Align, it suggests that Inter-Align improves cross-task geometric alignment by bringing adjacent task centroids closer and reducing global representational shift.

Mean Pairwise Cosine Distance. Centroid Cosine Distance reflects only the difference between task centroids, so it may miss finer distributional differences. We therefore compute Mean Pairwise Cosine Distance by averaging cosine distances over cross-task pairs:

$$d_{\text{pair}} = \mathbb{E}_{(\mathbf{z}_p, \mathbf{z}_c)}[1 - S(\mathbf{z}_p, \mathbf{z}_c)], \quad (28)$$

where $\mathbf{z}_p \in \mathcal{Z}_p$, and $\mathbf{z}_c \in \mathcal{Z}_c$.

This metric measures distribution level gap between previous and current tasks by averaging cosine distances over cross-task sample pairs. Lower

²<https://github.com/QData/TextAttack>

Table 6: Cross-attack results averaged over five attacks (PGD-5, PGD-10, FGSM, Rand, and discrete perturbations).

Model	AP(↑)	FGT(↓)	FWT-1(↑)	FWT-2(↑)	BWT(↑)
Sequence	37.47	8.78	2.20	1.61	-7.52
+ S (Smooth)	43.23	4.04	3.72	2.50	-1.68
+ C (Clip)	36.24	9.76	1.59	0.67	-7.87
+ A (Align)	39.33	5.14	1.67	-0.38	-3.46
+ S + C + A	44.22	2.76	3.48	2.90	-0.40
Replay	40.85	3.89	2.38	0.23	-1.81
+ S (Smooth)	45.75	2.61	5.15	4.39	-0.93
+ C (Clip)	41.39	4.13	1.23	0.99	-2.08
+ A (Align)	41.60	3.66	1.22	0.97	-1.80
EWC	36.61	10.12	1.60	1.21	-8.08
+ S (Smooth)	43.31	4.18	3.55	2.71	-1.83
+ C (Clip)	38.02	7.50	1.64	0.39	-5.40
+ A (Align)	36.76	8.83	2.17	0.29	-6.79
MoE	34.45	12.43	0.45	1.30	-10.78
+ S (Smooth)	35.73	9.25	1.41	-0.13	-7.92
+ C (Clip)	34.20	11.37	0.64	0.54	-10.17
+ A (Align)	35.23	10.48	1.40	0.71	-9.13

values mean the two tasks are closer on average at sample level. Therefore, a decrease after adding Inter-Align suggests improved cross-task geometric alignment by narrowing the distribution level gap, not only the centroid gap.

Directional Prototype Alignment. While the previous two metrics quantify centroid and distribution gaps, they do not indicate whether current task representations are aligned toward the previous task prototype. To capture this, we treat the previous task centroid $\hat{\mathbf{z}}_p$ as a prototype and measure how strongly current task representations align with it:

$$s_{c \rightarrow p} = \frac{1}{n_c} \sum_{j=1}^{n_c} S(\mathbf{z}_j^c, \hat{\mathbf{z}}_p). \quad (29)$$

This metric measures alignment strength from current task representations to previous task prototype. Larger $s_{c \rightarrow p}$ indicates stronger alignment, consistent with the intended effect of Inter-Align.

E.2 Results

For each adjacent task pair, Table 7 reports the absolute differences of three geometric metrics, computed as the difference between sequence training with Inter-Align enabled and sequence training without Inter-Align, using representations extracted after finishing training on each current task. We

denote these differences by Δd_{cent} , Δd_{pair} , and $\Delta s_{c \rightarrow p}$, respectively.

For Δd_{cent} and Δd_{pair} , a negative value indicates improvement because it means a reduced geometric gap. For $\Delta s_{c \rightarrow p}$, a positive value indicates improvement because it means current samples align more strongly with the previous task prototype in representation space.

Across adjacent task pairs, Inter-Align consistently reduces centroid gaps, since Δd_{cent} is negative for all pairs. For four of the five adjacent task pairs, it also reduces distribution level gaps and increases prototype alignment. These results support the claim that Inter-Align improves cross-task geometric alignment by narrowing representation gaps and pulling current task representations toward the previous task prototype.

For $xsum \rightarrow xlsun$, we observe a small inconsistency in that centroid gap is further reduced, whereas distribution level and alignment deltas take opposite signs compared with most adjacent task pairs. A plausible reason is that $xsum$ and $xlsun$ are highly similar, so centroid gap is already very small and Inter-Align mainly induces fine grained redistribution of representations, which can lead to small fluctuations at distribution level and in prototype alignment.

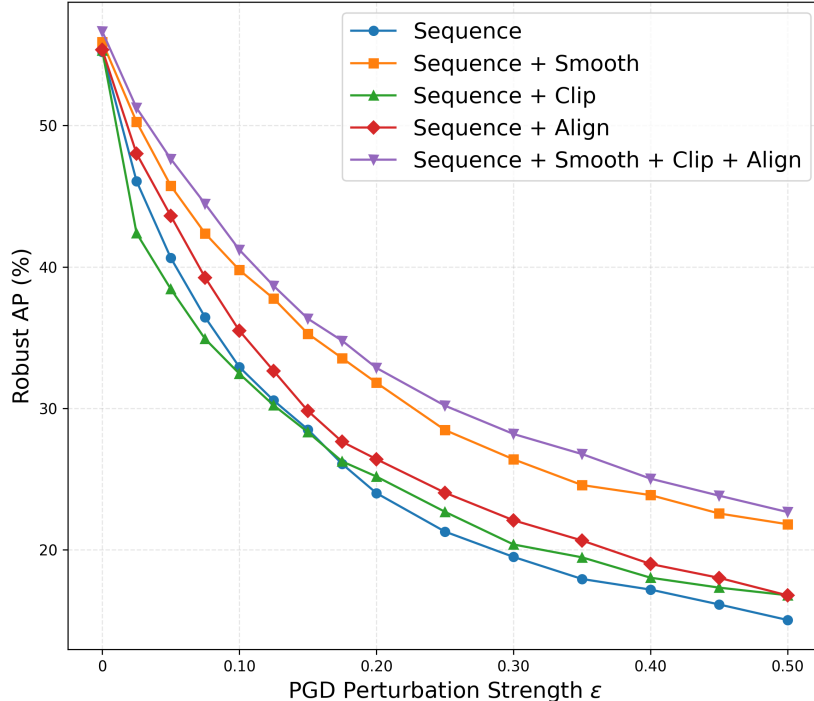


Figure 4: Robustness curve under PGD.

Table 7: Absolute differences of geometric metrics for adjacent task pairs, reported in percentage points, where $\Delta(\cdot) = (\cdot)_{\text{Sequence+Inter-Align}} - (\cdot)_{\text{Sequence}}$.

Task Pair	Δd_{cent}	Δd_{pair}	$\Delta s_{c \rightarrow p}$
anger \rightarrow emotion	-0.087	-0.065	+0.090
emotion \rightarrow agnews	-0.020	-0.168	+0.162
agnews \rightarrow anli	-0.086	-0.051	+0.063
anli \rightarrow xsum	-0.694	-1.087	+0.964
xsum \rightarrow xlsun	-0.144	+0.373	-0.051

F Additional Analysis of Inter-Align

F.1 Similarity Shift

We study how Inter-Align shifts cross-task similarity in representation space of a fixed encoder by applying directional perturbations to current task samples toward previous task prototype. Figure 5 shows that this perturbation increases cross-task similarity. As ϵ_{inter} increases, similarity gain rises and gradually saturates for both centroid and mean pairwise (distribution) similarity, indicating that Inter-Align improves similarity in a tunable way.

F.2 Inter-Align Sensitivity to Perturbation Strength

We study the sensitivity of Inter-Align to perturbation strength ϵ_{inter} on Sequence baseline. As shown in Table 8, Inter-Align consistently reduces forgetting across a wide range of ϵ_{inter} (e.g., FGT decreases from 3.42 to around 1.50–2.20) and improves backward transfer (BWT increases from -2.11 to as high as -0.69). These trends indicate that Inter-Align effectively stabilizes previously learned knowledge and alleviates catastrophic forgetting even when the alignment strength varies.

Meanwhile, AP is broadly stable across ϵ_{inter} , with only minor decreases. This is expected because Inter-Align acts as a cross-task geometric regularizer by pulling a subset of current representations toward previous task prototype, and it is not designed to explicitly improve performance on current task. Consequently, it can impose a mild constraint that prioritizes preserving past knowledge, which may slightly reduce AP while keeping changes small and acceptable.

Overall, these results suggest that Inter-Align is robust to the choice of ϵ_{inter} and serves as an effective plug-in module for mitigating forgetting and improving backward transfer, with minimal impact on average performance.

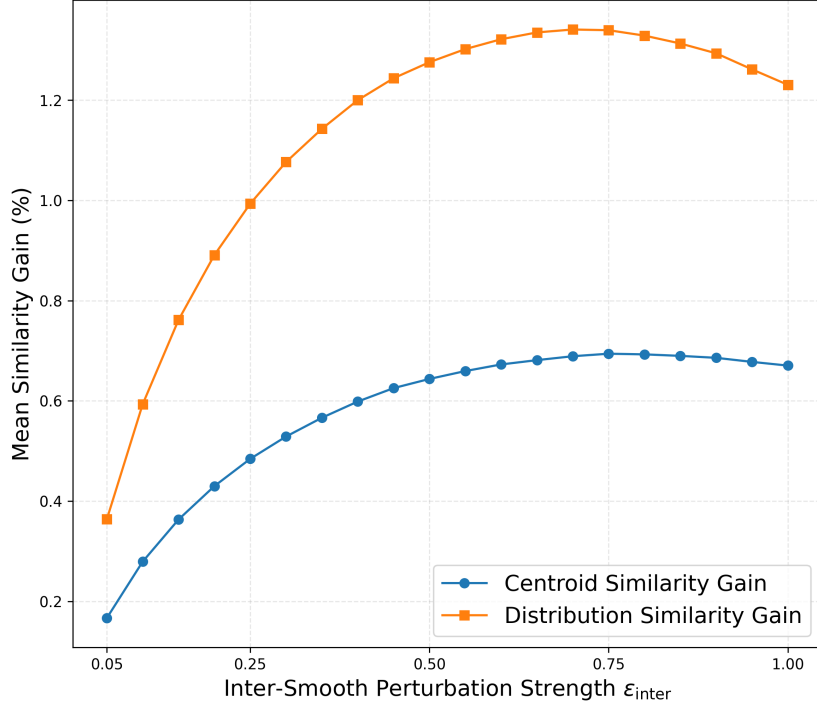


Figure 5: Similarity gain under varying ϵ_{inter} .

G Computational Overhead Analysis

We take one training step without any module enabled as the baseline computation (denoted as $1.0\times$), which consists of a standard forward and backward update. Below, we approximate additional computation by counting extra forward passes and gradient computations introduced by each module.

Intra-Smooth requires solving perturbation Δ_{intra}^* for a subset of samples. Specifically, to update Δ_{intra}^* (e.g., k_{intra} steps of PGD), we need extra forward passes and gradient computations to obtain ∇_{Δ} on the subset. Since this process is applied only to a fraction r_{intra} of the batch, additional computation can be approximated as $r_{\text{intra}}k_{\text{intra}}$. Under default settings $r_{\text{intra}}=0.25$ and $k_{\text{intra}}=1$, Intra-Smooth incurs approximately $+25\%$ ($1.25\times$) additional computation.

Inter-Align similarly solves directional perturbation Δ_{inter}^* on a fraction r_{inter} of the batch. Additional cost mainly comes from extra forward and gradient computations needed to update Δ_{inter}^* , yielding an overhead of approximately $r_{\text{inter}}k_{\text{inter}}$. Under default settings $r_{\text{inter}}=0.125$ and $k_{\text{inter}}=1$, Inter-Align incurs approximately $+12.5\%$ ($1.125\times$) additional computation.

Proto-Clip applies a similarity-based clipping

regularizer by comparing representations from the baseline training step with the previous task prototype. In implementation, this module reuses the intermediate activations from the baseline step and is backpropagated jointly with the main loss, without requiring an extra model forward or backward pass. Therefore, its additional cost is dominated by lightweight similarity and clipping operations and is negligible in practice.

H Additional Performance Analysis

H.1 Per-Task Stagewise Performance Curves

Figure 6 shows per-task stagewise performance curves. It can be observed that the three-module combination prioritizes long-term stability and cross-stage transfer rather than short-term optimality at each stage. Moreover, the improvements vary by task. On Tasks 1, 3, and 4, it yields more stable performance curves and maintains or even improves performance on earlier tasks in later stages, indicating stronger retention and potential positive backward transfer. For Task 5, while the performance is not particularly strong at the initial stage, it increases as stages progress. In contrast, the corresponding Sequence baseline shows a declining trend, suggesting that the benefits of our method may accumulate gradually over stages. Notably,

Table 8: Standard evaluation on Sequence baseline with Inter-Align under different perturbation strengths ϵ_{inter} . We mainly focus on forgetting (FGT) and backward transfer (BWT). Finer-grained ϵ_{inter} values show the same trend and are omitted.

Setting	AP(\uparrow)	FGT(\downarrow)	FWT-1(\uparrow)	FWT-2(\uparrow)	BWT(\uparrow)
Sequence ($\epsilon_{\text{inter}} = 0.00$)	55.21	3.42	1.65	1.76	-2.11
+ Inter-Align ($\epsilon_{\text{inter}} = 0.01$)	55.00	1.80	1.79	0.72	-1.11
+ Inter-Align ($\epsilon_{\text{inter}} = 0.02$)	54.86	1.62	1.52	0.25	-0.72
+ Inter-Align ($\epsilon_{\text{inter}} = 0.03$)	55.36	2.20	0.28	1.23	-1.29
+ Inter-Align ($\epsilon_{\text{inter}} = 0.04$)	55.00	1.50	1.66	0.50	-0.86
+ Inter-Align ($\epsilon_{\text{inter}} = 0.05$)	54.91	2.11	1.76	0.79	-1.31
+ Inter-Align ($\epsilon_{\text{inter}} = 0.10$)	54.84	2.14	1.78	0.84	-1.44
+ Inter-Align ($\epsilon_{\text{inter}} = 0.15$)	54.87	1.88	1.90	0.56	-1.08
+ Inter-Align ($\epsilon_{\text{inter}} = 0.20$)	54.94	1.80	1.92	0.83	-1.31
+ Inter-Align ($\epsilon_{\text{inter}} = 0.25$)	54.98	1.80	1.67	0.65	-1.05
+ Inter-Align ($\epsilon_{\text{inter}} = 0.30$)	55.46	2.10	1.84	0.83	-0.69

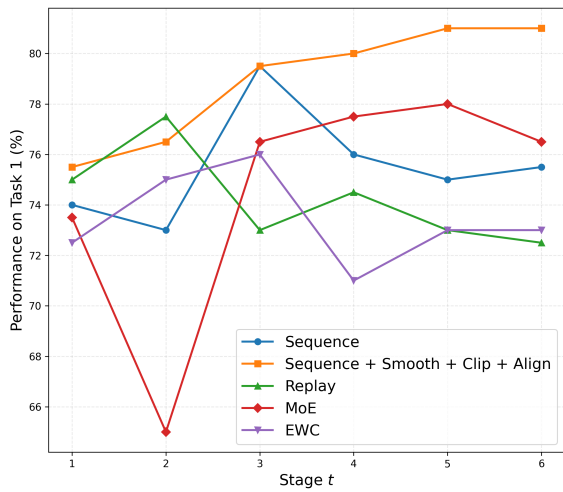
degradation on Task 2 (emotion) is not unique to our method. Except for Replay, most baselines exhibit a similar declining trend on this task, which we attribute to this task’s fine-grained semantic boundaries and its dependence on lexical sentiment markers (e.g., negation, intensifiers, and affective words). These properties make it more vulnerable to representation drift caused by learning subsequent tasks. Meanwhile, Replay’s advantage is consistent with sample rehearsal, which explicitly reinforces earlier decision boundaries.

H.2 Standard and Robust Performance Comparison

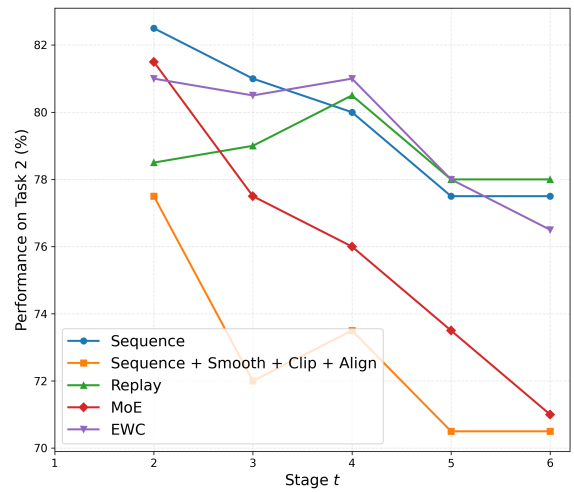
Figure 7 presents a two-dimensional view of different methods by jointly comparing standard average performance (Standard AP) and robust average performance (Robust AP) under two robustness settings. Overall, the relationship between Standard AP and Robust AP is not a simple trade-off. In particular, most baselines enhanced by our modules move toward the upper-right region, reflecting simultaneous improvements in both Standard AP and Robust AP. Note that Intra-Smooth, Proto-Clip, and Inter-Align are not designed with identical goals. Proto-Clip acts as a regularizer that limits over-alignment to the current task, while Align targets cross-task directional alignment. Nevertheless, under robustness settings these modules can still affect Robust AP, which often shifts the enhanced baselines upward while maintaining competitive Standard AP. At the same time, only a few outliers are observed, mostly under PGD (Input) setting.

When the three modules are combined with

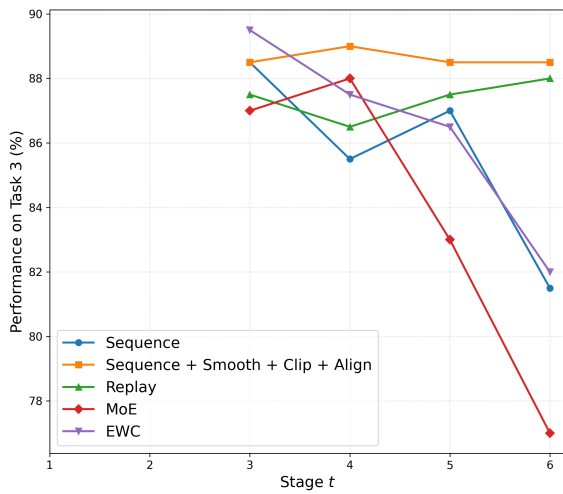
Sequence baseline, the resulting model achieves higher Standard AP than the corresponding baseline and exhibits a consistent improvement in Robust AP. Among all the models, it is surpassed only by two special settings, Replay + Intra-Smooth, which benefits from rehearsal samples, and Separate + Intra-Smooth, which trains each task independently. The former directly reinforces earlier tasks via explicit replay, whereas the latter is not subject to cross-task forgetting, placing both at a more advantageous position in this comparison.



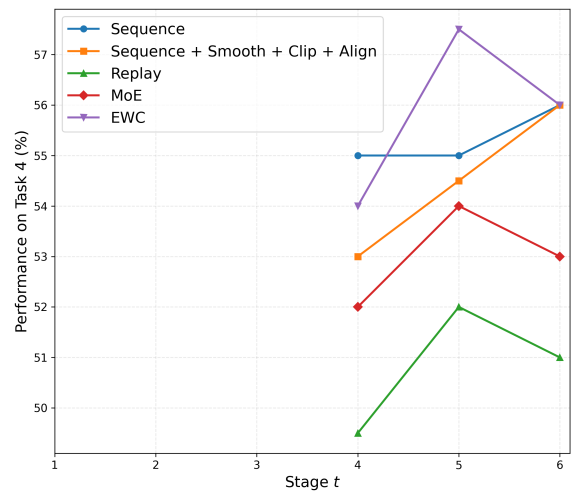
(a) Task 1 (anger)



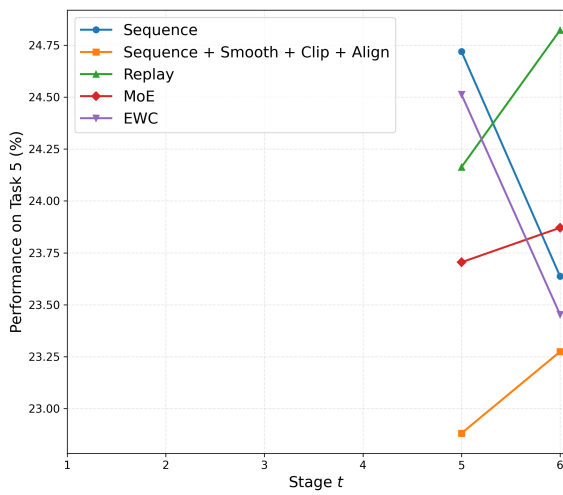
(b) Task 2 (emotion)



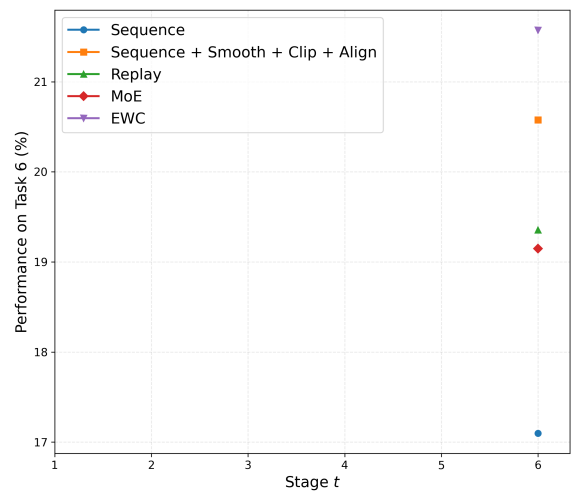
(c) Task 3 (agnews)



(d) Task 4 (anli)

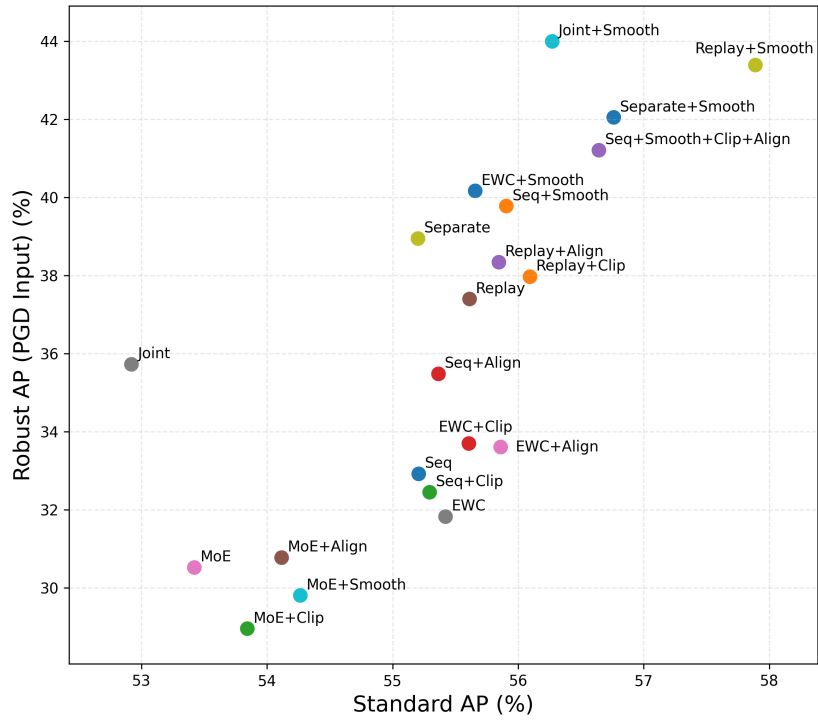


(e) Task 5 (xsum)

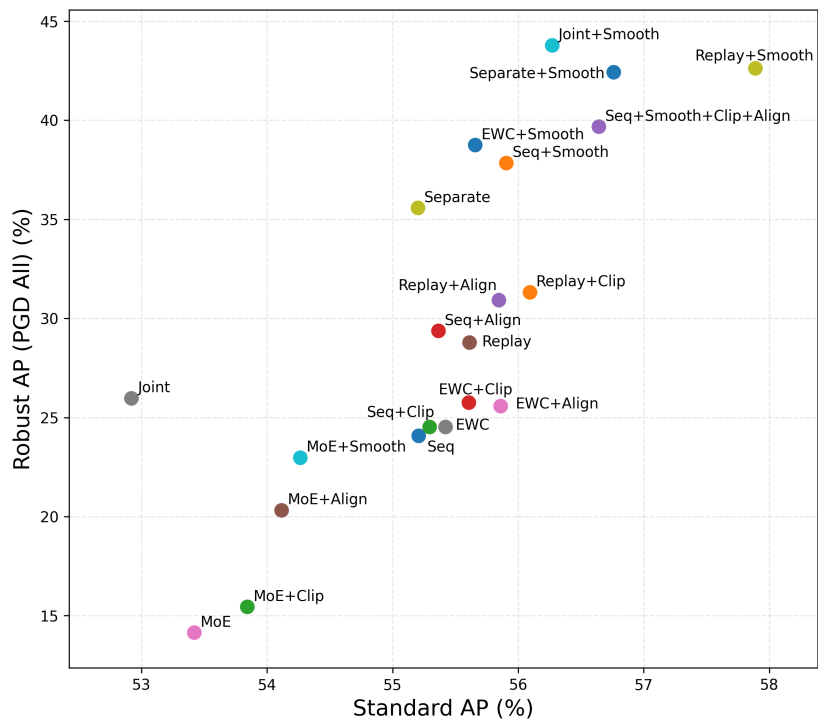


(f) Task 6 (xsum)

Figure 6: Per-task stagewise performance curves across all stages.



(a) PGD (Input)



(b) PGD (All)

Figure 7: Comparison between standard average performance and robust average performance under PGD attacks. PGD (Input) perturbs only input tokens, whereas PGD (All) perturbs both instruction and input tokens. Here, seq denotes the Sequence baseline.